

# Dual-Function Fluorescent Covalent Organic Frameworks: HCl Sensing and Photocatalytic H<sub>2</sub> Evolution from Water

Ahmed F. M. EL-Mahdy, Ahmed M. Elewa, Sheng-Wen Huang, Ho-Hsiu Chou,\* and Shiao-Wei Kuo\*

Two ultrastable luminescent covalent organic frameworks (COFs), PyTA-BC and PyTA-BC-Ph, are synthesized through polycondensations of 4,4',4'',4'''-pyrene-1,3,6,8-tetrayl)tetraaniline (PyTA-4NH<sub>2</sub>) with two carbazole-based derivatives having different degrees of conjugation. The PyTA-BC and PyTA-BC-Ph COFs exhibit ultrahigh thermal stabilities (up to 421 °C), excellent crystallinity, and high Brunauer–Emmett–Teller surface areas (up to 1445 m<sup>2</sup> g<sup>-1</sup>). These COFs display strong fluorescence emissions in various solvents, with their emission maxima gradually red-shifting upon increasing the polarity of the solvent (solvatochromism). Upon exposure to HCl, they respond very rapidly and sensitively in terms of changing their colors and fluorescence emission maxima. In the presence of a sacrificial electron donor, these COFs mediate the highly efficient photocatalytic evolution of H<sub>2</sub> from water. In the absence of a noble metal cocatalyst, the COFs and ascorbic acid provide a photocatalytic H<sub>2</sub> production of up to 1183 μmol g<sup>-1</sup> h<sup>-1</sup> (λ ≥ 420 nm); this value is the highest reported to date for a COF. Such COFs appear to be potentially useful as chemosensors for the naked-eye and sensitive spectroscopic detection of HCl and as cocatalysts for the sustainable photocatalytic production of H<sub>2</sub> from water.

present on earth, because it is less dense than air and, thus, escapes from our atmosphere.<sup>[1–3]</sup> Natural H is often combined with other compound elements, such as H<sub>2</sub>O, coal, and petroleum, and, thus, methods for the production of H<sub>2</sub> gas have so far been based on the isolation from natural gas, coal, petroleum, or water through electrolysis.<sup>[4]</sup> These traditional preparation techniques are constrained by associated CO<sub>2</sub> emissions and high energy consumption. Inexpensive techniques for efficient H<sub>2</sub> generation would, therefore, assist in sustaining our evolving H<sub>2</sub> economy. The splitting of water into H<sub>2</sub> and O<sub>2</sub> is a green and safe approach that has the potential to replace our high fossil fuel consumption—<sup>[5]</sup> especially sunlight-driven water splitting through photocatalytic reactions.<sup>[6,7]</sup> An optimal semiconductor for photocatalytic splitting of water into H<sub>2</sub> gas would have a bandgap suitable for absorbing solar light within the

## 1. Introduction

Hydrogen is the simplest—and one of the most abundant—elements on earth. Hydrogen as a gas, however, is not naturally

visible range and high stability in water; in addition, it should be nontoxic, plentiful, and easy to process into desired shapes.<sup>[8,9]</sup> Most inorganic photocatalysts are limited by their wide bandgaps (thereby absorbing photons within relatively short spans of wavelengths, leaving most of the solar spectrum inaccessible),<sup>[10]</sup> while organic semiconductors have rarely been investigated, even though they have many attractive properties (e.g., the capacity to absorb multiple photons, suitable ability to transport charge carriers, and, more particularly, diverse synthetic modularity for tailoring of these properties).<sup>[11]</sup> Graphene oxide, poly(*p*-phenylene), conjugated copolymers,<sup>[12–14]</sup> polymer Dots,<sup>[15,16]</sup> hydrophilic polymers,<sup>[17,18]</sup> metal–organic frameworks, and graphitic carbon nitride (g-C<sub>3</sub>N<sub>4</sub>, abbreviated as CN) have been investigated most widely as photocatalysts for the drive toward green and sustainable energy production. CN is a particularly promising metal-free photocatalyst for H<sub>2</sub> evolution because it is nontoxic, inexpensive, and highly chemically and thermally stable.<sup>[9–11,19]</sup> Nevertheless, the use of CN is limited by its insolubility in most organic solvents, its synthesis through polycondensation under harsh conditions, its high recombination rate of charge carriers at high temperature, its inability to absorb light at wavelengths greater than 460 nm, and its low electrical conductivity.<sup>[20]</sup> Furthermore, the CN molecular backbone features either triazine or heptazine components, thereby reducing its molecular tunability.


Covalent organic frameworks (COFs) have recently emerged as an exciting class of photoactive materials for light-driven H<sub>2</sub>

Prof. A. F. M. EL-Mahdy, S.-W. Huang, Prof. S.-W. Kuo  
Department of Materials and Optoelectronic Science  
Center of Crystal Research  
National Sun Yat-Sen University  
Kaohsiung 80424, Taiwan  
E-mail: kuosw@faculty.nsysu.edu.tw

Prof. A. F. M. EL-Mahdy  
Chemistry Department  
Faculty of Science  
Assiut University  
Assiut 71516, Egypt

A. M. Elewa, Prof. H.-H. Chou  
Department of Chemical Engineering  
National Tsing Hua University  
No. 101, Sec. 2, Kuang-Fu Rd., Hsinchu 30013, Taiwan  
E-mail: hhchou@mx.nthu.edu.tw

Prof. S.-W. Kuo  
Department of Medicinal and Applied Chemistry  
Kaohsiung Medical University  
Kaohsiung 807, Taiwan

 The ORCID identification number(s) for the author(s) of this article can be found under <https://doi.org/10.1002/adom.202000641>.

DOI: 10.1002/adom.202000641

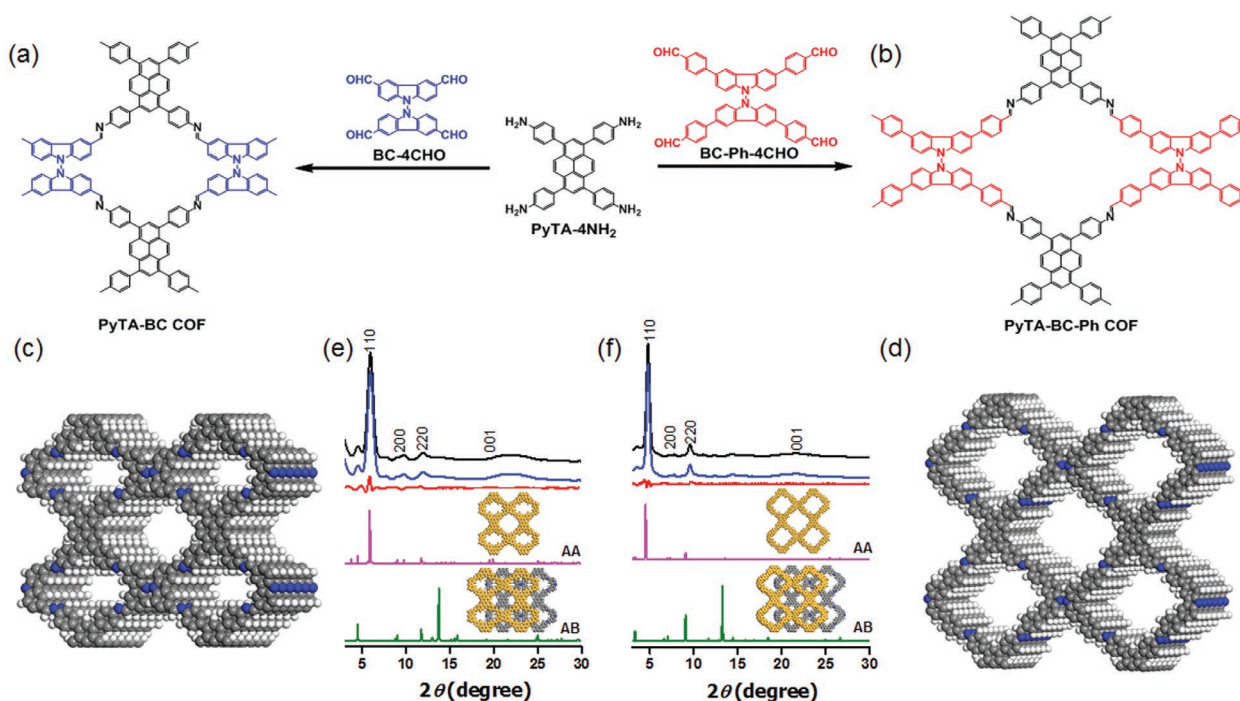


**Figure 1.** a–d) Schematic representation of the synthesis and top-view images of the a,c) PyTA-BC and b,d) PyTA-BC-Ph COFs in their AA stacking models. e,f) PXRD patterns of the e) PyTA-BC and f) PyTA-BC-Ph COFs: experimental patterns (black), simulated Pawley refined patterns (blue), their difference (red), and the simulated patterns obtained from the AA (purple) and AB (green) stacking models.

production, due to their tunable light-harvesting and charge-carrier properties.<sup>[21,22]</sup> COFs are lightweight, porous, crystalline materials constructed with strong covalent bonds among, typically, C, B, O, N, and Si atoms.<sup>[23–27]</sup> COFs have attracted considerable interest for their use in such applications as gas storage, adsorption, energy storage, separation, semiconducting materials, and catalysis, due to their low densities and  $\pi$ -stacked architectures.<sup>[28–40]</sup> Reversibility in the formation of covalent bonds during their network-forming reactions confers self-healing capacity to COFs, allowing repair of any structural defects and promoting the reorganization of their frameworks to provide long-range order and crystallinity.<sup>[41]</sup>

Herein, we report the syntheses of two ultrastable luminescent 2D COFs—PyTA-BC and PyTA-BC-Ph—having high Brunauer–Emmett–Teller (BET) surface areas (up to  $1445 \text{ m}^2 \text{ g}^{-1}$ ), through Schiff base formation under solvothermal conditions from 4,4',4'',4'''-pyrene-1,3,6,8-tetra(yl)tetraaniline (PyTA-4NH<sub>2</sub>) and two tetraformyl carbazole species having different conjugation lengths: 3,3',6,6'-tetraformyl-9,9'-bicarbazole (BC-4CHO) and 4,4',4'',4'''-(9,9'-bicarbazole)-3,3',6,6'-tetra(yl)trabenzaldehyde (BC-Ph-4CHO), respectively (Figure 1a,b). Because of their high surface areas, ultrahigh stability, and strong fluorescence efficiencies, these COFs functioned as sensitive chemosensors for HCl as well as photocatalysts for the evolution of H<sub>2</sub> from water.

## 2. Results and Discussion

Carbazole is a tricyclic aromatic heterocyclic compound that is highly stable toward chemical, thermal, and environmental

factors. Several carbazole-based compounds have received attention for their use as electronic and photoluminescent materials, because of the excellent charge-transporting and electron-donating properties of carbazole, in addition to the ease of post-functionalization of its structure at the N atom and on the aromatic carbon skeleton.<sup>[42–44]</sup> To exploit these attractive features of carbazole, we employed two carbazole-based linkers—BC-4CHO and BC-Ph-4CHO, having different conjugation lengths—for the preparation of two carbazole-based COFs, then investigated the effects of the conjugation length on the sensor behavior and photocatalytic H<sub>2</sub> production of these COFs. We obtained the COFs PyTA-BC and PyTA-BC-Ph after solvothermal Schiff base condensations of PyTA-4NH<sub>2</sub> (Figures S1–S3, Supporting Information) with BC-4CHO and BC-Ph-4CHO (Figures S4–S9, Supporting Information), respectively, in a mixture of *n*-butanol and *o*-dichlorobenzene (1:1) in the presence of acetic acid over 72 h at 120 °C (Figure 1a,b). Fourier transform infrared (FTIR) spectra of the PyTA-BC and PyTA-BC-Ph COFs (Figures S10 and S11, Supporting Information) revealed that the intensities of the stretching peaks for the N–H vibration band at  $3344 \text{ cm}^{-1}$  of PyTA-4NH<sub>2</sub> and the C=O vibration bands at  $1691 \text{ cm}^{-1}$  of BC-4CHO and BC-Ph-4CHO had been attenuated significantly. Furthermore, intense signals for imino bond (C=N) stretching appeared in the spectra of the PyTA-BC and PyTA-BC-Ph COFs at 1623 and  $1621 \text{ cm}^{-1}$ , respectively, confirming the success of the Schiff base condensations. Thermogravimetric analysis (TGA) of the PyTA-BC and PyTA-BC-Ph COFs revealed (Figure S12, Supporting Information) exceptional thermal stabilities, reaching as high as 421 °C under a N<sub>2</sub> atmosphere. The PyTA-BC-Ph COF having the longer conjugated system was the most stable, with a value

of  $T_{d5}$  of  $\approx 421$  °C and a char yield of 76%; for PyTA-BC COF, these values were 403 °C and 67%, respectively (Table S1, Supporting Information). Thus, increasing the conjugation length increased the thermal stability of the corresponding COF. Notably, these COFs had thermal stabilities superior to those of several recently reported 2D and 3D COFs, which had values of  $T_{d5}$  close to 250 °C.<sup>[21]</sup>

We used powder X-ray diffraction (PXRD) to investigate the crystallinity of our COFs (Figure 1c,d). The experimental PXRD pattern (Figure 1e, black curve) of the PyTA-BC COF featured a sharp first peak at a value of  $2\theta$  of 5.85°, which we assigned to the [110] reflection plane, as well as minor peaks at 9.03° and 11.95° attributed to the [200] and [220] reflection planes, respectively. We assigned the minor and broad peak that appeared at a value of  $2\theta$  of 22.01° to reflection from the [001] plane that occurred as a result of an extensive degree of  $\pi$ -stacking between the interlayers of the 2D PyTA-BC COF. The experimental PXRD pattern (Figure 1f, black curve) of the PyTA-BC-Ph COF featured a sharp peak at a value of  $2\theta$  of 4.75° for the [110] reflection plane, as well as a set of minor peaks at 7.30°, 9.36°, and 21.82°, which we attributed to the [200], [220], and [001] reflection planes, respectively. These PXRD patterns indicated that our new PyTA-BC and PyTA-BC-Ph COFs had microcrystalline frameworks and highly ordered 2D structures. We used the Bragg equation to determine the average  $d$ -spacing ( $d_{110}$ ) between the COF [110] planes and the distances between the stacked COF layers; for PyTA-BC and PyTA-BC-Ph COFs, the values of  $d_{110}$  were 1.51 and 1.85 nm, respectively, and the interlayer distances were 4.03 and 4.07 Å, respectively (Table S2, Supporting Information). These results indicated that the conjugation length of the tetraformyl building linker correlated well with the crystallinity of the resulting COF; that is, increasing the conjugation length of the linker increased the degree of planarity and, as we reported recently<sup>[28,29,45]</sup> increasing the planarity increased the crystallinity of the COFs (as measured in terms of their values of  $d_{110}$  and interlayer distances). Based on these findings, we used the Martial Studio package<sup>[46]</sup> to perform Pawley XRD refinements of the PyTA-BC and PyTA-BC-Ph COFs (Figure 1e,f, blue curves); the results were consistent with the experimental PXRD patterns (Figure 1e,f, black curves), as evidenced by very slight differences between them (Figure 1e,f, red curves). To obtain additional information about their 2D layer conformations and unit cell parameters, we constructed AA and AB stacking models of the PyTA-BC and PyTA-BC-Ph COFs. The theoretical XRD patterns obtained from the AA stacking models were highly consistent with the experimental ones (Figure 1e,f and Figures S13 and S14 (Supporting Information), purple curves), but they deviated significantly from the AB stacking models (Figure 1e,f, green curves). We obtained the following unit cell parameters from the AA stacking model of the PyTA-BC COF:  $a = 23.44$  Å;  $b = 19.62$  Å;  $c = 3.55$  Å;  $\alpha = \beta = \gamma = 90^\circ$ ; for the PyTA-BC-Ph COF:  $a = 27.41$  Å;  $b = 25.04$  Å;  $c = 4.18$  Å;  $\alpha = \beta = \gamma = 90^\circ$  (Figures S15 and S16, Tables S3 and S4, Supporting Information).

The  $^{13}\text{C}$  NMR spectra of the building blocks PyTA-4NH<sub>2</sub>, BC-4CHO, and BC-Ph-4CHO featured characteristic peaks at 148.21 (CNH<sub>2</sub>), 190.99 (CHO), and 193.80 (CHO) ppm, respectively (Figures S3, S6, and S9, Supporting Information). After solvothermal condensation of these units to form the PyTA-BC and

PyTA-BC-Ph COFs, these characteristic peaks were attenuated, with the solid state  $^{13}\text{C}$  NMR spectra featuring new signals at 156.86–157.97 ppm representing the C=N carbon atoms of the newly formed COFs (Figure 2a). We evaluated the permanent porosities of the PyTA-BC and PyTA-BC-Ph COFs through N<sub>2</sub> sorption isothermal analysis at 77 K. The adsorption/desorption curves of our new COFs (Figure 2b) were type I isotherms, corresponding to microporous materials. The BET surface areas of the PyTA-BC and PyTA-BC-Ph COFs, derived from their N<sub>2</sub> adsorption/desorption curves, were 520 and 1445 m<sup>2</sup> g<sup>-1</sup>, respectively, accompanied by pore volumes of 0.32 and 0.42 cm<sup>3</sup> g<sup>-1</sup>, respectively (Table S2, Supporting Information). It has been previously reported that the BET surface area of COF was strongly affected by the length of the building blocks; as the length of building block increased, the BET surface of the corresponding COF increased.<sup>[47,48]</sup> Thus, the PyTA-BC-Ph COF produced from the longer BC-Ph-4CHO unit exhibited much higher BET surface area than PyTA-BC produced from the shorter BC-4CHO. Moreover, we used non-local density functional theory (DFT) to estimate the pore size distributions of our COFs; the PyTA-BC and PyTA-BC-Ph COFs were microporous frameworks having two pore sizes of 1.09 and 1.57 nm for PyTA-BC COF and a single pore size of 1.92 nm for PyTA-BC-Ph COF (Figure 2c and Table S2, Supporting Information). To investigate the nanoscale morphologies of the PyTA-BC and PyTA-BC-Ph COFs, we recorded transmission electron microscopy (TEM) and field-emission scanning electron microscopy (FE-SEM) images after performing exfoliation in EtOH at room temperature for 1 h. Interestingly, the TEM images of the PyTA-BC COF revealed a well-defined dark homogenous spherical morphology, in contrast to uniformly loose block morphology of the PyTA-BC-Ph COF (Figure 2d,e and Figures S17 and S18, Supporting Information). Statistical calculations of these TEM images suggested that the spheres had an average diameter of  $\approx 400$ –450 nm, and that they were present as bunches, although some separated spheres were also observed, possibly due to exfoliation of PyTA-BC COF in EtOH during sample preparation. FE-SEM imaging also revealed the spherical and loose block morphologies of the PyTA-BC and PyTA-BC-Ph COFs, respectively (Figure 2f,g and Figure S19, Supporting Information). Thus, the conjugation lengths of the tetraformyl (BC-4CHO, BC-Ph-4CHO) building blocks controlled the morphologies of the resulting COFs. As the conjugation length increased, the planarity of the building block increased; again, as we reported recently,<sup>[28,29,45]</sup> the degree of planarity of the building block was the main characteristic affecting the morphology of the COF.

We investigated the photophysical behavior of our PyTA-BC and PyTA-BC-Ph COFs by recording their fluorescence emission spectra in solution. We dispersed the COFs in various solvents—acetone, tetrahydrofuran (THF), *N*-methyl-2-pyrrolidone (NMP), and dimethylformamide (DMF)—at a measuring concentration of 1 mg mL<sup>-1</sup>, and then excited the suspensions with light at a wavelength of 365 nm. The fluorescence spectra of the PyTA-BC COF in acetone, THF, NMP, and DMF (Figure 3a,b) featured emission maxima at 486, 464, 509, and 501 nm, respectively, while those of the PyTA-BC-Ph COF were 500, 461, 515, and 510 nm, respectively—that is, these two COFs had distinct fluorescence behavior. Moreover, the fluorescence spectra revealed that the emission maximum of each COF shifted to

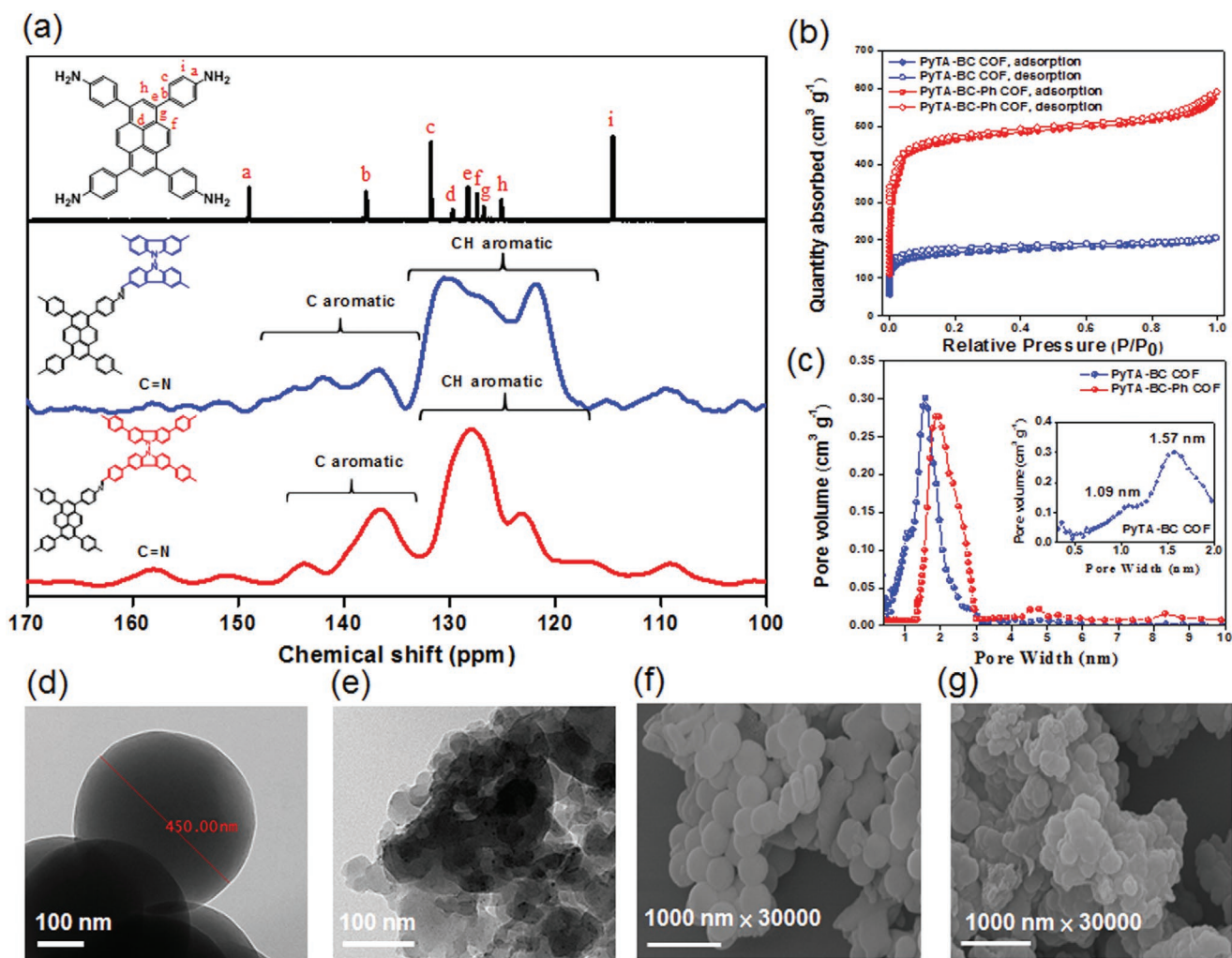


**Figure 2.** a) Solid state  $^{13}\text{C}$  CP/MAS NMR spectra, b)  $\text{N}_2$  sorption isotherms performed at 77 K, and c) pore size distributions of PyTA-4 $\text{NH}_2$  (black), PyTPA-BC (blue), and the PyTA-BC-Ph COF (red). d, e) TEM and f, g) SEM images of the d, f) PyTPA-BC and e, g) PyTA-BC-Ph COFs.

higher wavenumber upon increasing the polarity of the solvent (i.e., solvatochromism).<sup>[47]</sup> We assign this red-shifting of the fluorescence maximum to strong hydrogen bonding between the terminal  $\text{NH}_2$  groups on the COF surfaces and the  $\text{C}=\text{O}$  groups of the polar solvents acetone, NMP, and DMF. These hydrogen bonds would enhance the stability of the excited states of the COFs and, thus, accelerate intramolecular charge-transfer processes—a well-established solvent relaxation phenomenon and decrease the energy required for photoexcitation.<sup>[49–53]</sup> We ascribe the greater red-shifting of the signal for the PyTA-BC-Ph COF relative to that of the PyTA-BC COF to the longer conjugated length in the former. The fluorescence lifetime of the PyTA-BC COF was 3.56 ns, while that of the PyTA-BC-Ph COF was 3.89 ns. Furthermore, our synthesized COFs had excellent fluorescence stability, with their fluorescence emission intensities remaining approximately constant after keeping them in DMF for 60 days or after exciting them at 365 nm for 5 h (Figure 3c,d). Fluorescence images of the PyTA-BC and PyTA-BC-Ph COF suspensions (Figure 3e–h) revealed that their fluorescence colors were approximately green in the various solvents.

These features encouraged us to investigate the sensing properties of our COFs toward HCl. Interestingly, upon exposure to HCl gas, suspensions of the COFs ( $1 \text{ mg mL}^{-1}$ ) in DMF underwent color changes from yellow to red for the PyTA-BC COF and from yellow to brown for the PyTA-BC-Ph COF, indicating strong interactions between our synthesized COFs and HCl molecules (Figure 4a,b). In addition, these color changes were clearly evident to the naked eye and occurred with response times of less than 1 s—significantly faster than those of previously reported HCl sensors.<sup>[54–56]</sup> The red color of the PyTA-BC COF and the brown color of the PyTA-BC-Ph COF reverted back to their original yellow colors following exposure to  $\text{NH}_3$  vapor (Figure 4a,b). We observed no degradation in the color changes after 15 cycles of alternating exposure to HCl and  $\text{NH}_3$ , confirming the excellent reversibility and structural rigidity of the PyTA-BC and PyTA-BC-Ph COFs when used as HCl sensors. We evaluated the relationship between the fluorescence emissions of the suspended COFs in DMF and the concentration of HCl (Figure 4c,d). Upon the addition of a very small concentration of HCl ( $1 \text{ mmol L}^{-1}$ ), the intensities of the fluorescence emission maxima of the PyTA-BC and PyTA-BC-Ph COFs

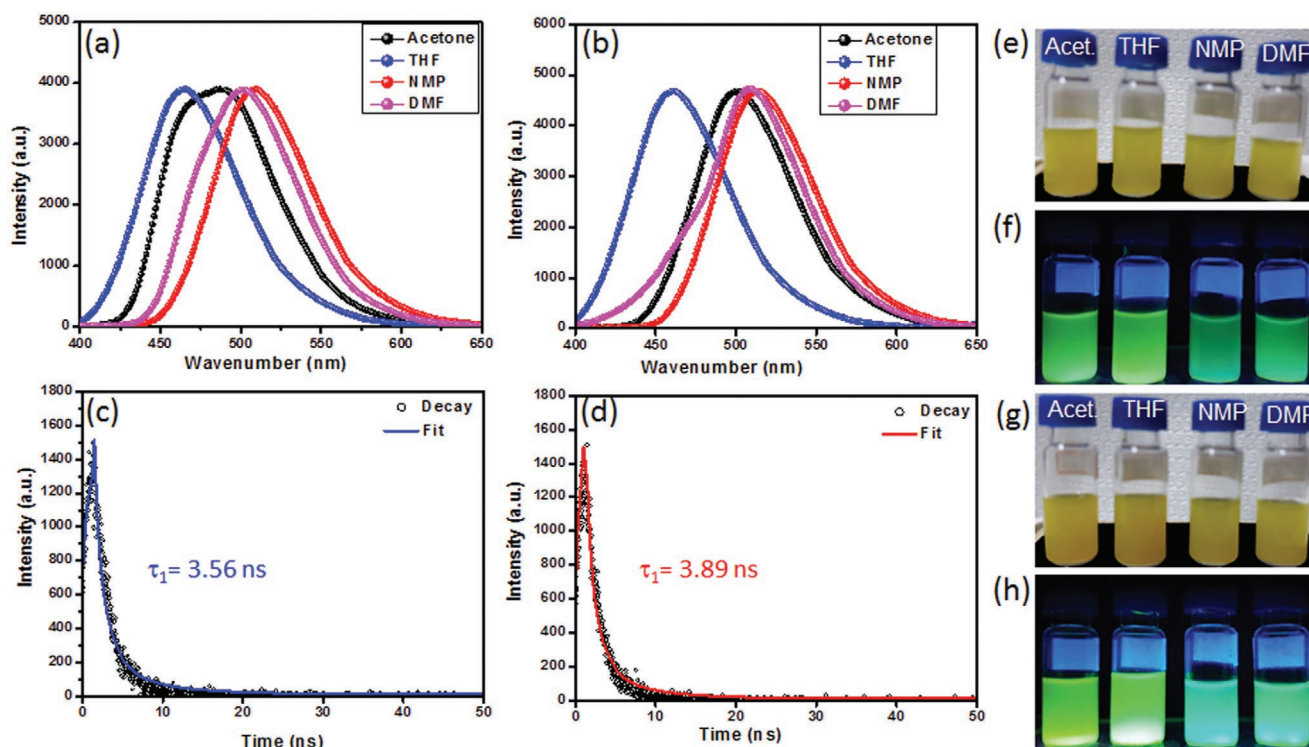


**Figure 3.** a,b) Fluorescence spectra of the a) PyTA-BC and b) PyTA-BC-Ph COFs as dispersions in various solvent (concentration:  $1 \text{ mg mL}^{-1}$ ; excitation wavelength:  $365 \text{ nm}$ ). c,d) Fluorescence life-time decays of the c) PyTA-BC and d) PyTA-BC-Ph COFs. e–h) Fluorescence images of the e,f) PyTA-BC and g,h) PyTA-BC-Ph COFs in DMF (concentration:  $1 \text{ mg mL}^{-1}$ ; excitation wavelength:  $365 \text{ nm}$ ).

at 501 and 510 nm, respectively, decreased significantly, and new emission peaks appeared at 598 and 611 nm, respectively. After the addition of HCl at a concentration of  $5 \text{ mmol L}^{-1}$ , the emission signals at 501 and 510 nm disappeared completely. The fluorescence emission signals at 598 and 611 nm increased gradually upon increasing the concentration of HCl from 1 to  $50 \text{ mmol}$ , but remained unchanged upon increasing the concentration of HCl thereafter. The calibration curves of the PyTA-BC and PyTA-BC-Ph COFs in the range of HCl concentrations from 1 to  $50 \text{ mmol L}^{-1}$ , with detection at 598 and 611 nm, respectively, revealed linear correlations ( $R^2 = 0.9840$  and  $0.9850$ , respectively), with lowest limits of detection of HCl of  $\approx 24$  and  $20 \text{ nmol L}^{-1}$ , respectively (Figure 4e,f). Figure 4g,h presents a possible sensing mechanism for the PyTA-BC and PyTA-BC-Ph COFs toward HCl. The imine nitrogen atoms in the COF skeletons would presumably undergo protonation under an HCl atmosphere, increasing the planarity of the PyTA-BC and PyTA-BC-Ph COFs by the formation of quinoid structures and, thereby, increasing the conjugation of the protonated COFs, leading to red-shifting of their fluorescence emissions (Figures S20, Supporting Information).<sup>[57–59]</sup> In addition, Ascherl et al. reported that the protonated imine ( $\text{C}=\text{NH}^+$ ) group is stronger electron-acceptors than its free imine ( $\text{C}=\text{N}$ ) group,<sup>[60]</sup> thus the  $\text{C}=\text{NH}^+$  groups in our COF skeletons after protonation would be accelerated the charge transfer process from the electron-donating carbazole moieties to the pyrene units, leading to the decreasing of the transition photoexcitation energies which causing this red-shifting. The reusability and recyclability of our PyTA-BC and PyTA-BC-Ph COFs as fluorescent

HCl sensors were investigated as shown in Figure S21 (Supporting Information). After the addition of HCl at a concentration of  $20 \text{ mmol L}^{-1}$ , the PyTA-BC and PyTA-BC-Ph COFs were recovered by the addition of a solution of trimethylamine in DMF ( $20 \text{ mmol L}^{-1}$ ) until the pH = 7. The intensities of the fluorescence emission maxima of our COFs non-significant decreased after six recovery cycles, suggesting the potential utilization of PyTA-BC and PyTA-BC-Ph COFs as HCl sensors. Moreover, the selectivity of our PyTA-BC and PyTA-BC-Ph COFs toward HCl was examined by the addition of various acids at a concentration of  $20 \text{ mmol L}^{-1}$  to the suspension solutions of our COFs. As shown in Figure S22 (Supporting Information), only HCl caused a significant red-shifting of fluorescence emission maxima of the PyTA-BC and PyTA-BC-Ph COFs to 598 and 611 nm, respectively, with very strong fluorescence emission intensities.

In the immediate past, a few fluorescent  $\beta$ -ketoenamine and imine-linked COFs have been reported as pH and gaseous HCl sensors. Zhang et al. reported the utilization of  $\beta$ -ketoenamine-linked COF-JLU4, which synthesized by the [3 + 2] polycondensation of 2,5-dimethoxyterephthalohydrazide with triformylphloroglucinol, as fluorescent pH sensor in aqueous solution.<sup>[61]</sup> Increasing the pH from 4.5 to 9.0 didn't effect on the fluorescence maximum of COF-JLU4, while increasing the pH from 9.0 to 13.0 associated with a gradually decreasing of the COF fluorescence intensity. In the acidic region, decreasing the pH from 4.5 to 0.9 led to increase the COF fluorescence intensity and shifting of the fluorescence emission maximum to lower wavelength. Therefore, comparing with our PyTA-BC

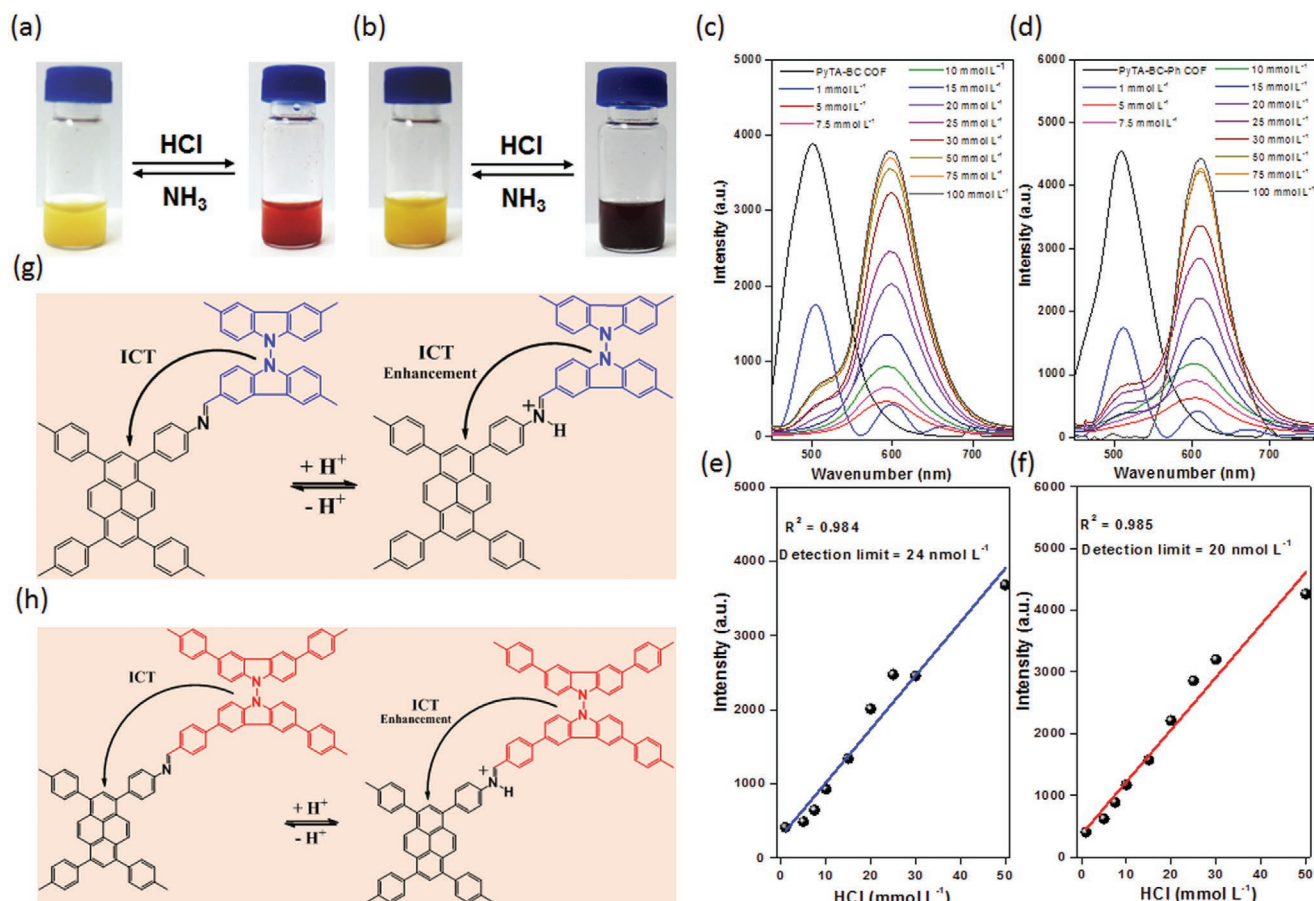


**Figure 4.** a,b) Optical photographs of the a) PyTA-BC and b) PyTA-BC-Ph COFs as dispersions in DMF ( $1 \text{ mg mL}^{-1}$ ) after exposure to HCl and  $\text{NH}_3$  vapors. c,d) Fluorescence spectra of the c) PyTA-BC and d) PyTA-BC-Ph COFs as dispersions in DMF (concentration:  $1 \text{ mg mL}^{-1}$ ; excitation wavelength:  $365 \text{ nm}$ ) in the presence of various concentrations of HCl. e,f) Calibration curves of the fluorescence intensities of the e) PyTA-BC and f) PyTA-BC-Ph COFs plotted with respect to the HCl concentration. g,h) Schematic representation of the mechanism of protonation and deprotonation of the g) PyTA-BC and h) PyTA-BC-Ph COFs after sequential exposure to HCl and  $\text{NH}_3$  vapors.

and PyTA-BC-Ph COFs, the fluorescence emission maximum of  $\beta$ -ketoenamine-linked COF-JLU4 showed a blue-shift from green fluorescent color (at  $\text{pH} = 7$ ) to blue fluorescent color (at  $\text{pH} = 1$ ) while our PyTA-BC and PyTA-BC-Ph COF showed red-shifting. On the other hand, Cui et al. reported the first fluorescent imine-linked ETBA-DAB COF as HCl sensor.<sup>[62]</sup> The ETBA-DAB COF was prepared by the  $[4 + 2]$  polycondensation of 4,4',4''-(ethane-1,1,2,2-tetrayl)tetrabenzaldehyde and 1,4-diaminobenzene and its suspension in dioxane exhibited two fluorescence emission peaks at 425 and 514 nm. With the addition of different concentrations of HCl solution in dioxane, the intensity of the fluorescence emission peak at 425 nm decreased with increasing the HCl concentration, while the peak at 514 nm totally disappeared and a new emission peak at 601 nm was appeared which its intensity increased with increasing the HCl concentration. The protonation capacity of ETBA-DAB COF reached a maximum at  $39 \text{ mmol L}^{-1}$ , indicating by slightly change in the intensity of emission peak at 601 nm with HCl concentration over than  $39 \text{ mmol L}^{-1}$ . Ascherl et al. reported the preparation of imine-linked Per-N COF through the  $[4 + 2]$  polycondensation of 2,5,8,11-tetrakis(4-aminophenyl)perylene and naphthalene dicarbaldehyde.<sup>[60]</sup>

The Per-N COF did not exhibit fluorescence properties and thus it was applied as a colorimetric sensor for the trifluoroacetic acid (TFA) vapor using the UV-vis spectroscopy. The detection limit of TFA using this kind of COF was as low as  $35 \mu\text{g L}^{-1}$ . Therefore, comparing with the reported imine-linked COFs, our PyTA-BC and PyTA-BC-Ph COFs represents the first  $[4 + 4]$  COFs acting as fluorescent sensor for HCl in gaseous and solution states. In addition, our COFs synthesized from the nitrogen-rich carbazole linkers which increased the protonation capacity over  $50 \text{ mmol L}^{-1}$  which higher than that of ETBA-DAB COF. Furthermore, the detection limits of PyTA-BC and PyTA-BC-Ph COFs more sensitive than the reported Per-N COF.

Next, we examined the strong fluorescence behavior of our synthesized PyTA-BC and PyTA-BC-Ph COFs through photocatalytic  $\text{H}_2$  production measurements. First, we measured the diffuse reflectance UV-vis spectra and photocurrents of the COFs (Figure 5a). The UV-vis absorption spectra of the PyTA-BC and PyTA-BC-Ph COFs featured absorption bands near 320–420 nm, suitable for absorbing visible light. The spectrum of the PyTA-BC-Ph COF featured a very slightly red-shifted absorption onset (Figure 5a) relative to that of the PyTA-BC COF, the result of the greater conjugation and delocalization

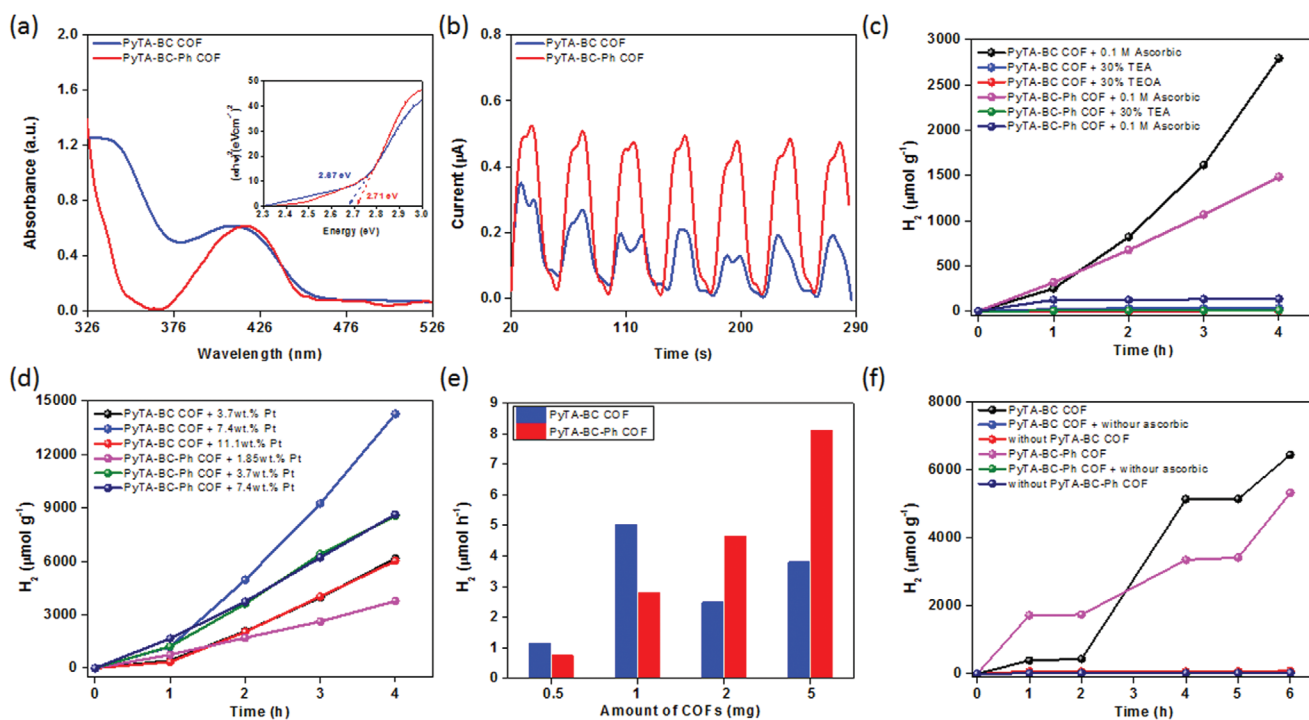


**Figure 5.** a) UV-vis absorption spectra of the PyTA-BC and PyTA-BC-Ph COFs in DMF, and their bandgaps calculated from Tauc plots. b) Photocurrents of the PyTA-BC and PyTA-BC-Ph COFs. c)  $H_2$  production rates plotted with respect to the amount of COFs. d) Effect of SEDs on the photocatalytic  $H_2$  production under visible light for the PyTA-BC and PyTA-BC-Ph COFs; 1 mg COFs in water/MeOH (2:1);  $\lambda > 420$  nm. e) Effect of the concentration of the cocatalyst on the photocatalytic  $H_2$  production under visible light for the PyTA-BC and PyTA-BC-Ph COFs; 1 mg COF in water/MeOH (2:1), 0.1 M ascorbic acid; UV cut-off filter ( $1000 \text{ W m}^{-2}$ ;  $\lambda \geq 420$  nm). f) Control experiments for photocatalytic  $H_2$  production under visible light for the PyTA-BC and PyTA-BC-Ph COFs; 1 mg COF in water/MeOH (2:1), 7.4 and 3.7 wt% Pt for PyTA-BC and PyTA-BC-Ph, respectively; 0.1 M ascorbic acid;  $\lambda > 420$  nm; ambient temperature.

that arose from  $\pi$ -stacking in the PyTA-BC-Ph COF. From Tauc plots, we estimated the optical bandgaps of the PyTA-BC and PyTA-BC-Ph COFs to be 2.71 and 2.67 eV, respectively (Figure 5a). The highest occupied molecular orbital (HOMO) energy was determined using a photoelectron spectrometer (Figure S23, Supporting Information) to be 5.62 and 5.72 eV for PyTA-BC and PyTA-BC-Ph COFs, respectively. The corresponding lowest unoccupied molecular orbital (LUMO) energy was calculated as  $E_{\text{HOMO}} - E_g$ , where  $E_g$  was determined from the Tauc plot method to be 2.91 and 3.05 eV. We speculate that our COFs will act as an efficient photocatalyst for light-driven hydrogen evolution because their lowest unoccupied molecular orbital (LUMO) positions are much higher than the potential of water reduction. The photocurrent of the PyTA-BC-Ph COF was larger than that of the PyTA-BC COF (Figure 5b). These findings suggest that separation and transfer of photogenerated electrons occurred in the COFs under illumination, and that these processes were more efficient in the PyTA-BC-Ph COF.

We examined the photocatalytic production of  $H_2$  mediated by our PyTA-BC and PyTA-BC-Ph COFs at ambient temperature under visible light ( $\lambda \geq 420$  nm) irradiation, with the hydrogen evolution rate (HER) measured using gas chromatography (GC). We tested triethylamine (TEA), triethanolamine (TEOA), and ascorbic acid as sacrificial electron donors (SEDs), and added MeOH to facilitate mixing of the immiscible COF/water system. In the initial test, no metal cocatalyst was added. The PyTA-BC and PyTA-BC-Ph COFs exhibited excel-

lent photocatalytic activities in the presence of ascorbic acid, with their HERs reaching 1183 and 417  $\mu\text{mol g}^{-1} \text{h}^{-1}$ , respectively (Figure 5c)—these values are higher than those of many other previously reported COFs.<sup>[22,63]</sup> (Figure 5c). The best performance was achieved by using ascorbic acid as the SED; the production of  $H_2$  when using TEA or TEOA was negligible (Figure 5c). Thereafter, we employed Pt and Pd as cocatalysts under our experimental conditions for  $H_2$  evolution. Decent performance (5030 and 2763  $\mu\text{mol g}^{-1} \text{h}^{-1}$ ) was achieved when using Pt as the cocatalyst for the PyTA-BC COF and PyTA-BC-Ph COFs, respectively (Figure S24, Supporting Information). As revealed in Figure 5d, the HERs for the photochemical reactions were highest when using 7.4 and 3.7 wt% Pt as a cocatalyst with the PyTA-BC and PyTA-BC-Ph COFs, respectively. Figure S25 (Supporting Information) displays the effect of various concentrations of ascorbic acid on the  $H_2$  evolution. Higher ascorbic acid concentrations decreased the HER for the PyTA-BC COF; a concentration of 0.1 M resulted in the maximum  $H_2$  production rate (Figure S25, Supporting Information). In contrast, higher ascorbic acid concentrations increased the HER for the PyTA-BC-Ph COF (Figure S25, Supporting Information). We investigated the effect of the amount of the PyTA-BC and PyTA-BC-Ph COFs on the  $H_2$  production rate (Figure 5e). As the amount of the PyTA-BC-Ph COF increased, the rate of  $H_2$  production increased (Figure 5e), presumably because its high surface area ( $1445 \text{ m}^{-2} \text{g}^{-1}$ ) increased the number of available active sites and the amount of light absorbed. In contrast,

the PyTA-BC COF, which had a low surface area ( $520 \text{ m}^2 \text{ g}^{-1}$ ), exhibited its maximum  $\text{H}_2$  production rate when present at 1 mg (Figure 5e). The  $\text{H}_2$  production rate of the PyTA-BC-Ph COF was higher than that of the PyTA-BC COF (Figure 5e), presumably because the red-shift of the onset of absorption (Figure 5a) allowed the former to capture more visible photons. In addition to the degree of light absorption, the surface area might also have been an important characteristic influencing the catalytic performance of the PyTA-BC-Ph COF. The corresponding apparent quantum yields at 420 nm for the PyTA-BC and PyTA-BC-Ph COFs reached as high as 1.46% and 1.83%, respectively (Figure S26, Supporting Information). Finally, control experiments revealed that, at room temperature, no reactions occurred in the dark, and that no  $\text{H}_2$  evolution was detected in the absence of the COFs or in the absence of ascorbic acid (Figure 5f). We compared to the reported photocatalytic efficiencies of COFs in recent works, which are summarized in Table S5 (Supporting Information) which revealed that our COFs one of the highest photocatalytic materials for the production of  $\text{H}_2$  from water.

### 3. Conclusion

We have synthesized two luminescent COFs—PyTA-BC and PyTA-BC-Ph—through [4 + 4] condensations of PyTA-4 $\text{NH}_2$  with two carbazole-based tetraaldehydes BC-4CHO and BC-Ph-4CHO having different degrees of conjugation. FTIR and solid state NMR spectroscopy confirmed the chemical structures of the resulting COFs, which exhibited ultrahigh thermal stability (up to 421 °C) and high BET surface areas (up to  $1445 \text{ m}^2 \text{ g}^{-1}$ ). The conjugation length controlled the degree of crystallinity of the resultant COFs: increasing the conjugation length in the linker increased the degree of planarity and, thereby, increased the surface area and value of  $d_{100}$  of the 2D COF. These COFs exhibited high fluorescence emissions in various solvents, with their emission maxima in the range 464–515 nm shifted to higher wavelengths upon increasing the polarity of the solvent (i.e., solvatochromism). We tested our COFs for their fluorescence emissions for HCl sensing and for their ability to mediate the photocatalytic evolution of  $\text{H}_2$  from water. The COFs were sensitive to HCl at concentrations of up to  $20 \text{ nmol L}^{-1}$ , and responded quickly (<1 s), accompanied by changes in the color and fluorescence emission. Moreover, the COFs mediated the highly efficient photocatalytic evolution of  $\text{H}_2$  from water in the presence of ascorbic acid as and SED. In the absence of any noble metal cocatalysts, these COFs provided HERs as high as  $1183 \mu\text{mol h}^{-1} \text{ g}^{-1}$  ( $\lambda > 420 \text{ nm}$ ). Thus, such COFs appear suitable for use as HCl chemosensors and as cocatalysts for the efficient photocatalytic production of  $\text{H}_2$  from water.

### 4. Experimental Section

**Synthesis of PyTA-BC COF:** In a 25 mL Schlenk storage tube, PyTA-4 $\text{NH}_2$  (80 mg, 0.14 mmol) and BC-4CHO (63 mg, 0.14 mmol) were dissolved in *n*-BuOH (4 mL) and *o*-dichlorobenzene (4 mL) in the presence of AcOH (6 M, 0.8 mL). The tube was sealed and degassed through three freeze/pump/thaw cycles. The tube was sealed off by flame and heated at 120 °C for 3 days. After cooling to room temperature,

the tube was opened and the precipitate filtered off and washed two times each with *n*-BuOH, THF, and acetone. The solid was dried under vacuum at 120 °C overnight to afford a yellow powder (92%).

**Synthesis of PyTA-BC-Ph COF:** In a 25 mL Schlenk storage tube, PyTA-4 $\text{NH}_2$  (60 mg, 0.10 mmol) and BC-Ph-4CHO (79 mg, 0.10 mmol) were dissolved in *n*-BuOH (4 mL) and *o*-dichlorobenzene (4 mL) in the presence of AcOH (6 M, 0.8 mL). The tube was sealed and degassed through three freeze/pump/thaw cycles. The tube was sealed off by flame and heated at 120 °C for 3 days. After cooling to room temperature, the tube was opened and the precipitate filtered off and washed two times each with *n*-BuOH, THF, and acetone. The solid was dried under vacuum at 120 °C overnight to afford a yellow powder (90%).

**Photocatalytic  $\text{H}_2$  Evolution Experimental:** The photocatalytic experiments were performed in a 35 mL Pyrex reactor. The reactor was closed using rubber septa. In a typical photocatalytic reaction, a COF powder (1 mg) was dispersed in water/MeOH (2:1, 10 mL) containing 0.1 M ascorbic acid and  $\text{H}_2\text{PtCl}_6$  (7.4 and 3.7 wt% Pt for the PyTA-BC and PyTA-BC-Ph COFs, respectively). The suspension was purged with Ar for 5 min to remove dissolved air. The sample was then irradiated by a 350 W Xe lamp equipped with a UV cut-off filter ( $1000 \text{ W m}^{-2}$ ;  $\lambda \geq 420 \text{ nm}$ ); the reaction temperature was fixed at 25 °C using a flow of cooling water. The formation of  $\text{H}_2$  was confirmed by injecting a portion of the reactor headspace gas (0.5  $\mu\text{L}$ ) into a gas chromatograph (GC7920), operated under isothermal conditions using a semi-capillary column (molecular sieve; diameter: 8 mm; length: 3 m) equipped with a thermal conductivity detector.

**Quantum Efficiency Measurements:** A catalyst solution was prepared by dispersing a COF powder (1 mg) in water/MeOH (2:1, 10 mL) containing 0.1 M ascorbic acid and  $\text{H}_2\text{PtCl}_6$  (7.4 and 3.7 wt% Pt for PyTA-BC and PyTA-BC-Ph COFs, respectively). The catalyst solution was irradiated for 1 h by light from a 300 W Xe lamp ( $1000 \text{ W m}^{-2}$ ;  $\lambda \geq 420 \text{ nm}$ ) passed through a 420 nm band-pass filter. The formation of  $\text{H}_2$  was quantified using a gas chromatograph (GC7920), operated under isothermal conditions using a semi-capillary column (molecular sieve; diameter: 8 mm; length: 3 m) equipped with a thermal conductivity detector. The AQY was calculated as follows

$$\text{AQY} = \frac{\text{number of evolved } \text{H}_2 \text{ molecules} \times 2}{\text{number of incident photons}} \times 100\% \quad (1)$$

$$\begin{aligned} \text{AQY} &= \frac{N_e}{N_p} \times 100\% = \frac{2M \times N_A}{\frac{E_{\text{total}}}{E_{\text{photon}}}} \times 100\% = \frac{2M \times N_A}{S \times P \times t \times \frac{h \times c}{\lambda}} \times 100\% \\ &= \frac{2M \times N_A \times h \times c}{S \times P \times t \times \lambda} \times 100\% \end{aligned} \quad (2)$$

where  $M$  is the amount of  $\text{H}_2$  molecules (mol),  $N_A$  is the Avogadro constant ( $6.022 \times 10^{23} \text{ mol}^{-1}$ ),  $h$  is the Planck constant ( $6.626 \times 10^{-34} \text{ J s}$ ),  $c$  is the speed of light ( $2.997 \times 10^8 \text{ m s}^{-1}$ ),  $S$  is the irradiation area ( $\text{cm}^2$ ),  $P$  is the intensity of the irradiating light ( $\text{W cm}^{-2}$ ),  $t$  is the photoreaction time (s), and  $\lambda$  is the wavelength of the monochromatic light (m).

### Supporting Information

Supporting Information is available from the Wiley Online Library or from the author.

### Acknowledgements

This study was supported financially by the Ministry of Science and Technology, Taiwan, under contracts MOST 108-2218-E-110-013-MY3, 108-2638-E-002-003-MY2, 108-2218-E-110-013-MY3, and 108-2221-E-110-014-MY3. The authors also thank Mr. Hsien-Tsan Lin of the Regional



Instruments Center at National Sun Yat-Sen University for help with the TEM measurement.

## Conflict of Interest

The authors declare no conflict of interest.

## Keywords

covalent organic frameworks, H<sub>2</sub> evolution, luminescence, sensors

Received: April 15, 2020

Revised: May 26, 2020

Published online: June 15, 2020

- [1] B. Zohuri, *Hydrogen Energy: Challenges and Solutions for a Cleaner Future*, Springer, New York **2018**.
- [2] C. Kahraman, G. Kayakutlu, *Energy Management—Collective and Computational Intelligence with Theory and Applications*, Studies in Systems, Decision and Control, Vol. 149, Springer, New York **2018**.
- [3] J. Jayakumar, H.-H. Chou, *ChemCatChem* **2020**, *12*, 689.
- [4] S. S. Kumar, V. Himabindu, *Mater. Sci. Energy Technol.* **2019**, *2*, 442.
- [5] J. Wang, G. Ouyang, Y. Wang, X. Qiao, W. S. Li, H. Li, *Chem. Commun.* **2020**, *56*, 1601.
- [6] P. Kumar, R. Boukherroub, K. Shankar, *J. Mater. Chem. A* **2018**, *6*, 12876.
- [7] L. Cheng, Q. Xiang, Y. Liao, H. Zhang, *Energy Environ. Sci.* **2018**, *11*, 1362.
- [8] R. Saravanan, F. Gracia, A. Stephen, in *Nanocomposites for Visible Light-Induced Photocatalysis* (Eds: M. M. Khan, D. Pradhan, Y. Sohn), Springer, Cham **2017**, pp. 19–40.
- [9] X. Wang, K. Maeda, A. Thomas, K. Takanabe, G. Xin, J. M. Carlsson, K. Domen, M. Antonietti, *Nat. Mater.* **2009**, *8*, 76.
- [10] D. Friedmann, A. F. Lee, K. Wilson, R. Jalili, R. A. Caruso, *J. Mater. Chem. A* **2019**, *7*, 10858.
- [11] L. Li, Z. Cai, Q. Wu, W. Y. Lo, N. Zhang, L. X. Chen, L. Yu, *J. Am. Chem. Soc.* **2016**, *138*, 7681.
- [12] L.-Y. Ting, J. Jayakumar, C.-L. Chang, W.-C. Lin, M. H. Elsayed, H.-H. Chou, *J. Mater. Chem. A* **2019**, *7*, 22924.
- [13] A. Thomas, T. Appidi, A. B. Jogdand, S. Ghar, K. Subramaniyam, G. Prabhusankar, J. R. Mohanty, A. K. Rengan, *ACS Appl. Polym. Mater.* **2020**, *2*, 1388.
- [14] M. Rafiq, Z. Chen, H. Tang, Z. Hu, X. Zhang, Y. Xing, Y. Li, F. Huang, *ACS Appl. Polym. Mater.* **2020**, *2*, 12.
- [15] P.-J. Tseng, C.-L. Chang, Y.-H. Chan, L.-Y. Ting, P.-Y. Chen, C.-H. Liao, M.-L. Tsai, H.-H. Chou, *ACS Catal.* **2018**, *8*, 7766.
- [16] C.-L. Chang, W.-C. Lin, C.-Y. Jia, L.-Y. Ting, J. Jayakumar, M. H. Elsayed, Y.-Q. Yang, Y.-H. Chan, W.-S. Wang, C.-Y. Lu, *Appl. Catal., B* **2020**, *268*, 118436.
- [17] Y. Bai, Z. Hu, J.-X. Jiang, F. Huang, *Chem. - Asian J.* **2020**, <https://doi.org/10.1002/asia.202000247>.
- [18] R. S. Sprick, K. J. Cheetham, Y. Bai, J. A. Fernandes, M. Barnes, J. W. Bradley, A. I. Cooper, *J. Mater. Chem. A* **2020**, *8*, 7125.
- [19] B. Kumru, V. Molinari, M. Hilgart, F. Rummel, M. Schäffler, B. V. Schmidt, *Polym. Chem.* **2019**, *10*, 3647.
- [20] Z. Zhou, Y. Zhang, Y. Shen, S. Liu, Y. Zhang, *Chem. Soc. Rev.* **2018**, *47*, 2298.
- [21] X. Wang, L. Chen, S. Y. Chong, M. A. Little, Y. Wu, W. H. Zhu, R. Clowes, Y. Yan, M. A. Zwijnenburg, R. S. Sprick, A. I. Cooper, *Nat. Chem.* **2018**, *10*, 1180.
- [22] B. P. Biswal, H. A. Vignolo-González, T. Banerjee, L. Grunenberg, G. Savasci, K. Gottschling, B. V. Lotsch, *J. Am. Chem. Soc.* **2019**, *141*, 11082.
- [23] A. P. Cote, A. I. Benin, N. W. Ockwig, M. O’Keeffe, A. J. Matzger, O. M. Yaghi, *Science* **2005**, *310*, 1166.
- [24] P. J. Waller, F. Gándara, O. M. Yaghi, *Acc. Chem. Res.* **2015**, *48*, 3053.
- [25] W. Zhao, L. Xia, X. Liu, *CrystEngComm* **2018**, *20*, 1613.
- [26] H. R. Abuzeid, A. F. M. EL-Mahdy, S. W. Kuo, *Microporous Mesoporous Mater.* **2020**, *300*, 110151.
- [27] M. G. Mohamed, A. F. M. EL-Mahdy, M. M. M. Ahmed, S. W. Kuo, *ChemPlusChem* **2019**, *84*, 1767.
- [28] A. F. M. El-Mahdy, C. H. Kuo, A. Alshehri, C. Young, Y. Yamauchi, J. Kim, S. W. Kuo, *J. Mater. Chem. A* **2018**, *6*, 19532.
- [29] A. F. M. El-Mahdy, C. Young, J. Kim, J. You, Y. Yamauchi, S. W. Kuo, *ACS Appl. Mater. Interfaces* **2019**, *11*, 9343.
- [30] C. J. Doonan, D. J. Tranchemontagne, T. G. Glover, J. R. Hunt, O. M. Yaghi, *Nat. Chem.* **2010**, *2*, 235.
- [31] N. Huang, X. Chen, R. Krishna, D. Jiang, *Angew. Chem., Int. Ed.* **2015**, *54*, 2986.
- [32] A. F. M. El-Mahdy, Y. H. Hung, T. H. Mansoure, H. H. Yu, T. Chen, S. W. Kuo, *Chem. - Asian J.* **2019**, *14*, 1429.
- [33] A. F. M. EL-Mahdy, M. G. Mohamed, T. H. Mansoure, H. H. Yu, T. Chen, S. W. Kuo, *Chem. Commun.* **2019**, *55*, 14890.
- [34] Y. Song, Q. Sun, B. Aguila, S. Ma, *Adv. Sci.* **2019**, *6*, 1801410.
- [35] M. S. Kim, W. J. Lee, S. M. Paek, J. K. Park, *ACS Appl. Mater. Interfaces* **2018**, *10*, 32102.
- [36] X. H. Xiong, Z. W. Yu, L. L. Gong, Y. Tao, Z. Gao, L. Wang, W. H. Yin, L. X. Yang, F. Luo, *Adv. Sci.* **2019**, *6*, 1900547.
- [37] H. Yang, H. Wu, Z. Yao, B. Shi, Z. Xu, X. Cheng, F. Pan, G. Liu, Z. Jiang, X. Cao, *J. Mater. Chem. A* **2018**, *6*, 583.
- [38] S. Y. Ding, J. Gao, Q. Wang, Y. Zhang, W. G. Song, C. Y. Su, W. Wang, *J. Am. Chem. Soc.* **2011**, *133*, 19816.
- [39] C. Montoro, D. Rodríguez-San-Miguel, E. Polo, R. Escudero-Cid, M. L. Ruiz-González, J. A. Navarro, P. Ocón, F. Zamora, *J. Am. Chem. Soc.* **2017**, *139*, 10079.
- [40] H. R. Abuzeid, A. F. M. EL-Mahdy, M. M. M. Ahmed, S. W. Kuo, *Polym. Chem.* **2019**, *10*, 6010.
- [41] S. Yang, W. Hu, X. Zhang, P. He, B. Pattengale, C. Liu, M. Cendejas, I. Hermans, X. Zhang, J. Zhang, J. Huang, *J. Am. Chem. Soc.* **2018**, *140*, 14614.
- [42] B. Wex, B. R. Kaafarani, *J. Mater. Chem. C* **2017**, *5*, 8622.
- [43] M. Meier, L. Ji, J. Nitsch, I. Krummenacher, A. Deifsenberger, D. Auerhammer, M. Schäfer, T. B. Marder, H. Braunschweig, *Chem. - Eur. J.* **2019**, *25*, 4707.
- [44] T. Nishimoto, T. Yasuda, S. Y. Lee, R. Kondo, C. Adachi, *Mater. Horiz.* **2014**, *1*, 264.
- [45] A. F. M. EL-Mahdy, Y. H. Hung, T. H. Mansoure, H. H. Yu, Y. S. Hsu, K. C. Wu, S. W. Kuo, *J. Taiwan Inst. Chem. Eng.* **2019**, *103*, 199.
- [46] Accelrys Software Inc., Material Studio Modeling Environment, Release v7.0, San Diego: Accelrys Software Inc., **2013**.
- [47] H. Furukawa, O. M. Yaghi, *J. Am. Chem. Soc.* **2009**, *131*, 8875.
- [48] S. Feng, H. Xu, C. Zhang, Y. Chen, J. Zeng, D. Jiang, J. Jiang, *Chem. Commun.* **2017**, *53*, 11334.
- [49] K. Kalyanasundaram, J. K. Thomas, *J. Am. Chem. Soc.* **1977**, *99*, 2039.
- [50] E. M. S. Castanheira, J. M. G. Martinho, *Chem. Phys. Lett.* **1991**, *185*, 319.
- [51] S. Haldar, D. Chakraborty, B. Roy, G. Banappanavar, K. Rinku, D. Mullangi, P. Hazra, D. Kabra, R. Vaidhyanathan, *J. Am. Chem. Soc.* **2018**, *140*, 13367.
- [52] H. L. Qian, C. Dai, C. X. Yang, X. P. Yan, *ACS Appl. Mater. Interfaces* **2017**, *9*, 24999.
- [53] L. Ascherl, E. W. Evans, M. Hennemann, D. D. Nuzzo, A. G. Hufnagel, M. Beetz, R. H. Friend, T. Clark, T. Bein, F. Auras, *Nat. Chem.* **2018**, *9*, 3802.

- [54] Y. Y. Lv, J. Wu, Z. K. Xu, *Sens. Actuators, B* **2010**, *148*, 233.
- [55] M. Hu, W. Kang, B. Cheng, Z. Li, Y. Zhao, L. Li, *Microchim. Acta* **2016**, *183*, 1713.
- [56] M. Hu, W. Kang, Z. Zhong, B. Cheng, W. Xing, *Ind. Eng. Chem. Res.* **2018**, *57*, 11668.
- [57] Y. Z. Xie, G. G. Shan, Z. Y. Zhou, Z. M. Su, *Sens. Actuators, B* **2013**, *177*, 41.
- [58] P. Muthukumar, S. A. John, *Sens. Actuators, B* **2011**, *159*, 238.
- [59] W. F. Jager, T. S. Hammink, O. van den Berg, F. C. Grozema, *J. Org. Chem.* **2010**, *75*, 2169.
- [60] L. Ascherl, E. W. Evans, J. Gorman, S. Orsborne, D. Bessinger, T. Bein, R. H. Friend, F. Auras, *J. Am. Chem. Soc.* **2019**, *141*, 15693.
- [61] Y. Zhang, X. Shen, X. Feng, H. Xia, Y. Mu, X. Liu, *Chem. Commun.* **2016**, *52*, 11088.
- [62] F. Z. Cui, J. J. Xie, S. Y. Jiang, S. X. Gan, D. L. Ma, R. R. Liang, G. F. Jiang, X. Zhao, *Chem. Commun.* **2019**, *55*, 4550.
- [63] P. Pachfule, A. Acharjya, J. Roeser, T. Langenhahn, M. Schwarze, R. Schomäcker, J. Schmidt, *J. Am. Chem. Soc.* **2018**, *140*, 1423.